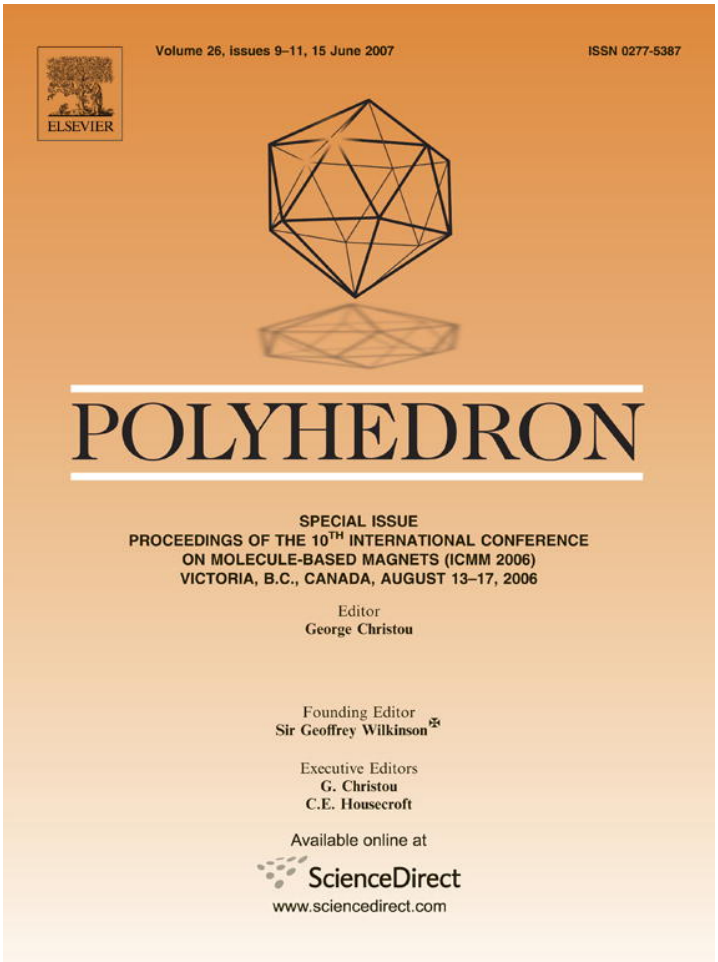

Available online at www.sciencedirect.com
ScienceDirect
Polyhedron 26 (2007) 2225–2229
POLYHEDRON
www.elsevier.com/locate/poly

High-frequency EPR characterization of a triangular Mn_3 single-molecule magnet

Sheng-Chiang Lee [a], Theocharis C. Stamatatos [b], Stephen Hill [a,*], Spyros P. Perlepes [b], George Christou [c]

[a] Department of Physics, University of Florida, Gainesville, FL 32611, USA
[b] Department of Chemistry, University of Patras, 26504 Patras, Greece
[c] Department of Chemistry, University of Florida, Gainesville, FL 32611, USA

Received 28 September 2006; accepted 24 October 2006
Available online 17 November 2006

Abstract

We present the results of a multi-high-frequency single-crystal EPR study of a recently discovered triangular trinuclear Mn complex, $[Mn_3O(O_2CMe)_3(mpko)_3](ClO_4)\cdot 3CH_2Cl_2$. The obtained data set confirm the findings of earlier magnetic measurements, which suggested that this complex is a single-molecule magnet with a spin ground state of $S = 6$. The zero-field splitting parameters obtained from the present EPR study are: $D = -0.3\ cm^{-1}$, $B_4^0 = -3 \times 10^{-5}\ cm^{-1}$ and $g = 2.00$. We also find a significant transverse anisotropy which can be parameterized by a rhombic distortion with an E value of at least $0.015\ cm^{-1}$.

Keywords: Single-molecule magnets; Nanomagnet; Electron paramagnetic resonance; Quantum tunneling; Manganese

1. Introduction

It has been a widely held view that triangular single-molecule magnets (SMMs) would never exist, because all known examples of such triangular complexes exhibited antiferromagnetic exchange interactions within the magnetic core, leading to small spin quantum numbers [1–3]. However, Stamatatos et al. recently succeeded in synthesizing the first triangular SMM, $[Mn_3O(O_2CMe)_3(mpko)_3](ClO_4)\cdot 3CH_2Cl_2$ (hereon abbreviated Mn_3), by introducing relatively small, ligand-imposed structural distortions which alter the exchange interactions from being antiferromagnetic to ferromagnetic [1]. In this communication, we present the results of a multi-high-frequency single-crystal EPR study which confirms the findings of previous magnetic measurements—namely, that Mn_3 is a SMM possessing a significant ground state spin quantum number of $S = 6$ and an appreciable negative magneto-crystalline anisotropy parameterized by a D value of $-0.3\ cm^{-1}$ [1].

2. Experimental

The complex was synthesized through the reaction of $[Mn_3O(O_2CMe)_6(py)_3](ClO_4)$ with methyl 2-pyridyl ketone oxime (mpkoH) in $MeOH/MeCN/CH_2Cl_2$, resulting in dark-brown crystals of Mn_3 (labeled **2** in Ref. [1]). The Mn^{III} ions are ferromagnetically coupled in a near-equilateral triangular configuration. Unfortunately, the molecules do not align in parallel in the lattice, but fall into two groups whose magnetic axes are separated by approximately 69.7°, as illustrated in Fig. 1. Previous low-temperature magnetization/susceptibility studies of this complex revealed SMM-like behavior [1], including hysteresis and frequency dependent peaks in the out-of-phase AC susceptibility.

* Corresponding author. Tel.: +1 352 392 5711.
E-mail address: hill@phys.ufl.edu (S. Hill).

0277-5387/$ - see front matter © 2006 Elsevier Ltd. All rights reserved.
doi:10.1016/j.poly.2006.10.052

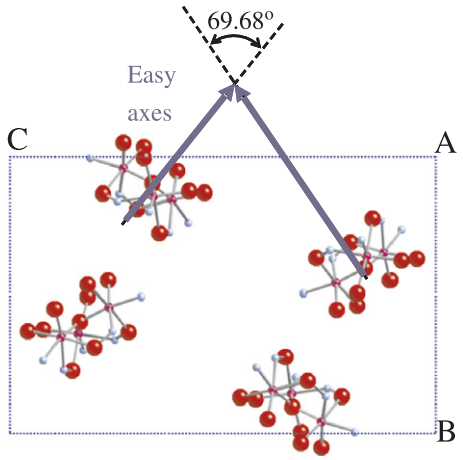

Fig. 1. Crystal structure showing the two sites in the lattice with differently oriented magnetic axes.

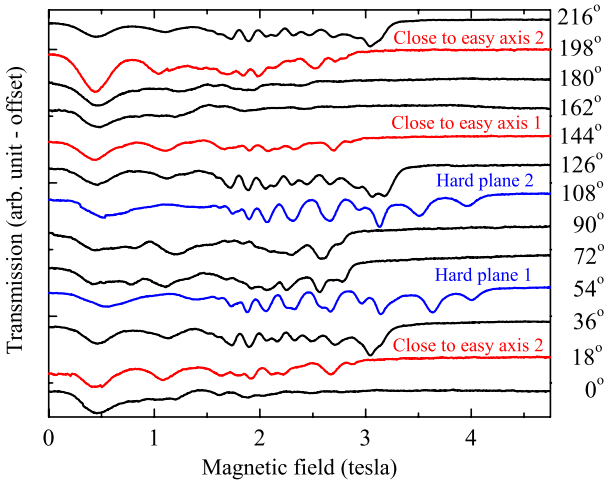

Fig. 2. Angle-dependent spectra taken at 62 GHz and 5 K; the angles are given on the right hand side. The blue curves correspond to the directions of the two hard planes. The red curves correspond to the closest approaches to the two easy axes. (For interpretation of the references in color in this figure legend, the reader is referred to the web version of this article.)

In this work, we perform high-frequency electron paramagnetic resonance (HFEPR) measurements to quantitatively determine the zero-field-splitting (zfs) parameters in the spin Hamiltonian based on the giant spin approximation [4]. HFEPR measurements were performed at various temperatures and frequencies from 60 to 170 GHz, with magnetic fields applied at different orientations relative to a single crystal. The HFEPR spectra were obtained at fixed frequencies and temperatures while varying the DC magnetic field strength. Details of the experiments can be found elsewhere [5]. These studies allow us to identify the ground state spin quantum number and to construct the Zeeman diagram associated with this state. By comparing the experimentally constructed Zeeman diagram to simulations obtained via exact diagonalization of the spin Hamiltonian, the zfs parameters can be determined quantitatively.

3. Data and discussion

The HFEPR study of this complex is complicated due to the existence the two inequivalent sites in the lattice, with differently oriented magnetic axes, neither of which align with the principal crystallographic axes (see Fig. 1). Shown in Fig. 2 are the angle-dependent spectra taken at 62 GHz and 5 K. The appearance of multiple peaks spanning a wide field range is indicative of a molecular species with an appreciable spin quantum number and significant anisotropy [6]. If one assumes an easy axis type of anisotropy (negative D value), then one expects to see the strongest peaks appearing at low fields when the field is aligned near to the easy axis, while the strongest peaks should appear at high fields when the field is in the hard plane. Clearly, the data in Fig. 2 exhibit both of these behaviors.

Since the orientation of the crystal was not known a priori, we do not know the exact plane of rotation relative to either the crystallographic axes or the magnetic axes associated with the two sites in the lattice. However, for rotation over more than a 180° angle range, we are guaranteed to pass through the hard planes associated with both sites (not necessarily coincidentally); we are also likely to pass close to the easy axes, but it is not guaranteed that we will hit those directions exactly. As can be seen from the coloring of the curves in Fig. 2, there exist two field orientations (54° and 108°, colored blue) exhibiting essentially identical spectra, with strong EPR peaks extending to the highest fields. These orientations, which are separated by about 50° (see Fig. 4 below), correspond to the two hard planes associated with each lattice site. The fact that the obtained separation is less than the ~70° separation of the easy axes confirms that the plane of field rotation is inclined relative to the plane containing the two easy axes. Nevertheless, we do expect to pass close to the easy axes for field orientations 90° away from the hard planes, i.e. 18°, 144° and 198°. One can indeed see from these traces (colored in red) that the spectra do resemble easy axis data at low fields, i.e. broader, well spaced peaks decreasing in strength with increasing field [7]; the cluster of small peaks at higher fields originate from the other species.

Fig. 3 shows an expanded view of the 54° data in Fig. 2. At high fields, one clearly sees two series of more-or-less evenly spaced peaks marked by blue squares and red arrows. The highest field series (blue squares) correspond to the main peaks associated with one of the hard planes; the field is exactly in the hard plane for these sites (species 1). Meanwhile, the field is ~50° from the other hard plane, i.e. ~40° from the easy axis associated with the other sites (species 2). For such an orientation, one expects to observe remanences of both the easy axis spectrum (strong low-field peaks) and the hard plane spectrum (strong peaks at moderately high fields). The second series of closely spaced high-field peaks (marked by red arrows) and the two broad peaks at low fields (marked by black dots) correspond to the second species. The peaks marked by the red arrows

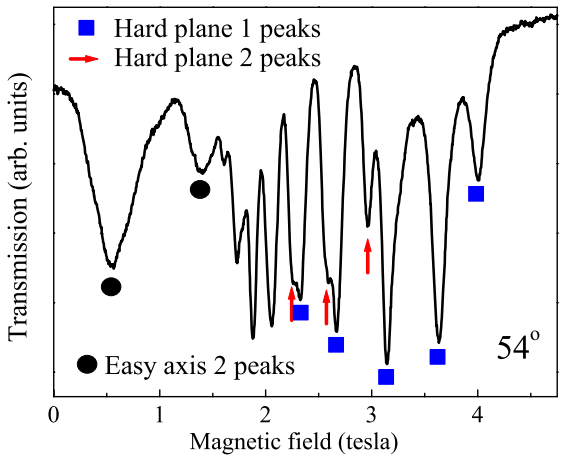

Fig. 3. An expanded view of the 54° data from Fig. 2 (field ‖ hard plane 1). The blue squares mark the resonances corresponding to the field parallel to hard plane 1 (species 1). The remaining resonances are due to the second species: the low-field peaks marked with black dots are remnants of the easy axis spectra, while the higher field peaks marked with red arrows are remnants of the hard plane spectra (see text). The field is oriented approximately 42° away from the easy axis of the second species. (For interpretation of the references in color in this figure legend, the reader is referred to the web version of this article.)

occur at lower fields than those marked by the blue squares because the field is significantly out of the hard plane for the second species.

Angle dependent measurements were also performed at a frequency of 129 GHz. Fig. 4 displays the angle dependence of the strongest peak positions. For a uniaxial system (easy axis or easy plane) in the high-field limit, $g\mu_B B \gg DS$ (= 2 T), one expects each peak to approximately follow a $(1 - 3\cos^2\theta)$ angle dependence about the isotropic position ($g = 2$ line), where θ is the orientation of the field relative to the principal (z-) axis (not the experimental angle from Fig. 4). As can be seen from the figure, each peak does

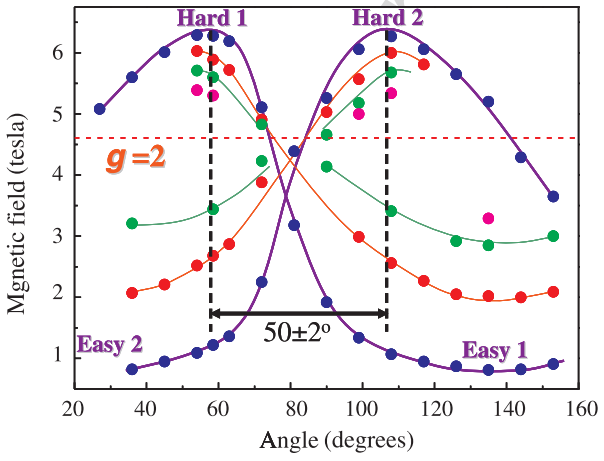

Fig. 4. EPR peak positions plotted vs. angle extracted from data obtained at a higher frequency of 129 GHz; the temperature is 5 K. Each peak exhibits an asymmetric twofold pattern (180° periodicity). The hard and easy directions are indicated in the figure for each species. The $g = 2$ line for a frequency of 129 GHz is also shown as a guide.

oscillate about $g = 2$. Furthermore, as expected, the deviation to the low-field side (field close to z-direction) of $g = 2$ is roughly twice the deviation to the high field side (field ‖ xy-plane) for each transition. The solid curves through the data points were generated by hand. Assuming D to be negative (see below), the locations of the two hard planes (dashed vertical lines) were estimated from the maxima of the blue curves.

There are multiple reasons for the departure from a perfect $(1 - 3\cos^2\theta)$ angle dependence seen in Fig. 4. First, when the field is near to the easy axis, the $g\mu_B B \gg DS$ condition is not satisfied; this causes sharper maxima and broader minima. Second, the field rotation plane is not orthogonal to the two hard planes, i.e. it does not coincide with the two easy axes. Consequently, there is a variation in the in-plane field component for each species as the magnetic field is rotated. Thus, the data in Fig. 4 provide the first evidence for transverse (in-plane) anisotropy. If there was no in-plane anisotropy, one would expect the angle dependence to be symmetric about the hard plane directions. This is clearly not the case, i.e. for hard plane 1, the fall off in the position of the peak is much sharper to the right of the hard plane than to the left (vice versa for hard plane 2). Consequently, there must be two anisotropies at play, one which depends only on the out-of-plane field component which is symmetric about the hard plane, and another that depends only on the in-plane field component, which need not necessarily be symmetric about the hard plane (this depends on the orientations of the hard and medium axes relative to the intersection between the hard plane and the field rotation plane).

In order to quantify the zfs parameters, frequency dependent measurements were performed with the magnetic field applied within the hard plane of one of the species of molecules, corresponding to 54° in Fig. 2 (hard plane 1). The positions of the observed resonances are plotted in the frequency versus field plot displayed in Fig. 5. We limited this analysis to the highest field series of evenly spaced peaks which we associate with the hard plane of one of the species (1), i.e. those marked by blue squares in Fig. 3, together with the strongest low-field peaks which we associate with the other species (2). We then simultaneously fit each series of peak positions to the usual spin Hamiltonian [4], using identical zfs parameters, since the two lattice sites are related by a simple rotation. We made the assumption that $S = 6$. However, similar attempts to fit the data were made with larger and smaller S values, and the quality of the best fits were significantly worse. In other words, the data plotted in Fig. 5 appear to confirm the spin quantum number of $S = 6$ deduced from magnetic measurements [1].

The red and blue curves in Fig. 5 correspond to the frequency differences between Zeeman split levels which differ in m_s by ±1, i.e. levels between which there are allowed magnetic dipole transitions. The red curves were fit to the red low-field data points and the blue curves to the high-field blue data points. We made the assumption that the

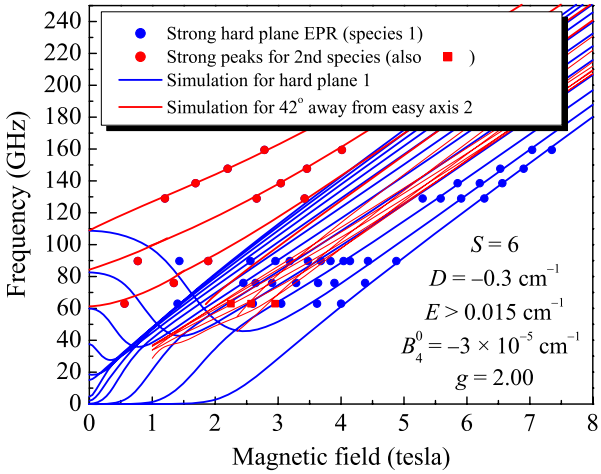

Fig. 5. Frequency dependence of the main EPR peaks observed at 5 K for the field applied parallel to hard plane 1 (54°). The solid blue circles correspond to species 1 and the solid red circles to the low-field peaks associated with species 2; the solid red squares correspond to the peaks marked by red arrows in Fig. 3. The curves represent the best fit to both data sets, yielding the zfs parameters given in the figure. The blue curves correspond DC fields applied in the hard plane for species 1, and red curves for fields applied 42° away from the easy axis associated with species 2. (For interpretation of the references in color in this figure legend, the reader is referred to the web version of this article.)

field was exactly in the hard plane for the blue curves, while the orientation of the field was adjusted for the red curves. The red data place the strongest constraint on the axial D and B_4^0 parameters, as well as determining the orientation of the field relative to the easy axis of the second species. In order to maintain a good fit to the low-field data, whilst simultaneously fitting the blue data points, we found it necessary to include a significant transverse anisotropy. Since we do not know the exact plane of rotation, we cannot determine the precise value of the transverse anisotropy parameter. Furthermore, we cannot determine its symmetry, as has been done for other SMMs via field rotation studies within the hard plane [8,9]. Nevertheless, to get some idea of the degree of transverse anisotropy, we use the standard rhombic interaction of the form $E(\widehat{S}_x^2 - \widehat{S}_y^2)$ [4].

The optimum fits to the data in Fig. 5 yield: $S = 6$, $D = -0.3\ \mathrm{cm}^{-1}$, $B_4^0 = -3 \times 10^{-5}\ \mathrm{cm}^{-1}$, $g = 2.00$ and a significant $E \geqslant 0.015\ \mathrm{cm}^{-1}$. For the second species, the field is found to be $42° \pm 2°$ away from the easy axis ($48° \pm 2°$ away from the hard plane), which agrees with the angle dependent measurements. The reason for the lower bound on E is because our fits assumed that the field was precisely along the hard axis for the high field data points (species 1, blue data points). One could include a larger E value and rotate the field slightly towards the medium axis (within the hard plane) and obtain an equally good fit. To place this in context, an E/D ratio of 0.05 is about a quarter of that found for the biaxial Fe_8 SMM [7,10]. Therefore, the transverse anisotropy is fairly significant.

Also seen in Fig. 5 are a series of thinner red curves which overlap the lower field blue curves. These red lines correspond to the higher field peaks expected of the second species (marked by red arrows in Fig. 3). We did not consider these peaks when fitting the data. However, three data points (red squares) are included in Fig. 5 corresponding to the peaks marked by red arrows for the 62 GHz data in Fig. 3. As can be seen, the locations of these peaks agree reasonably well with the thinner red curves in Fig. 5. Thus, the earlier explanation for these peaks appears to be sound. The slight deviations between the red square positions and the thin red curves may be attributed to the fact that we do not know the precise orientation of the field within the hard plane, i.e. one does not expect perfect agreement due to the uncertainty in the E value.

Finally, Fig 6 displays 129 GHz data obtained at 10 K and 5 K with the field parallel to the hard plane of species 1. The two insets display the Zeeman diagrams generated using the obtained zfs parameters for two field orientations: 42° away from the easy axis (left) and parallel to the hard plane (right). The red bars in these insets represent the observed EPR transitions. As can be seen from the figure, the EPR intensity transfers to the lowest and highest field peaks upon lowering the temperature, i.e. the transitions from the lowest lying levels in the two Zeeman diagrams. This behavior can only be explained assuming a negative D value. We note that changing the sign of D would not affect the fits displayed in Fig. 5. However, changing the sign of D would invert the Zeeman diagrams. Were this the case, one would expect the EPR intensity to shift to intermediate fields (around $g = 2$) upon lowering the temperature. Consequently, the temperature depen-

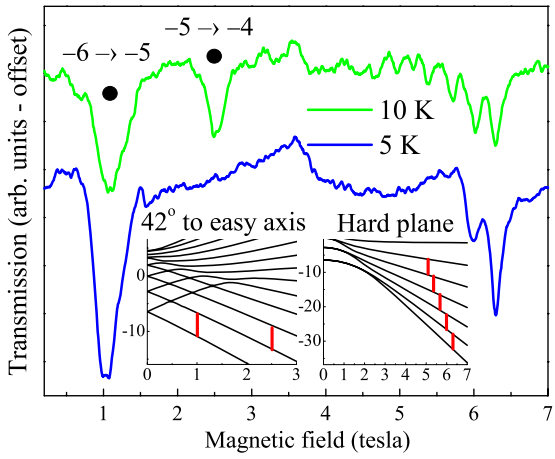

Fig. 6. Temperature dependence of the 129 GHz spectra obtained with the field parallel to hard plane 1 (54°). The two insets display the Zeeman diagrams generated using the obtained zfs parameters for two field orientations: 42° away from the easy axis (left) and parallel to the hard plane (right). The red bars in these insets represent the observed EPR transitions. The low-field transitions have been labeled according to the m_s values involved in the transitions. (For interpretation of the references in color in this figure legend, the reader is referred to the web version of this article.)

dence provides spectroscopic confirmation of a negative D value, thereby verifying that Mn_3 is in fact a SMM.

4. Summary

Multi-high-frequency single-crystal EPR measurements have enabled a quantitative determination of the zfs parameters of the first triangular Mn SMM. The obtained parameters are in good agreement with previously published values deduced from thermodynamic measurements, thereby providing spectroscopic evidence that Mn_3 is indeed a SMM.

Acknowledgement

This work was supported by the US National Science Foundation under grant numbers DMR-0239481 and DMR-0506946.

References

[1] Theocharis C. Stamatatos et al., J. Am. Chem. Soc. 127 (2005) 15380.
[2] J.B. Vincent, H.-R. Chang, K. Folting, J.C. Huffman, G. Christou, D.N. Hendrickson, J. Am. Chem. Soc. 109 (1987) 5703.
[3] G. Rajaraman, J. Brockman, M. Murugesu, C.E. Sanudo, J. Raftery, S.J. Teat, W. Wernsdorfer, G. Christou, E.K. Brechin, D. Collison, Chem.-Eur. J. 10 (2004) 5180.
[4] D. Gatteschi, R. Sessoli, Angew. Chem. 42 (2003) 268.
[5] S. Takahashi, S. Hill, Rev. Sci. Instrum. 76 (2005) 023114.
[6] S. Hill, J.A.A.J. Perenboom, N.S. Dalal, T. Hathaway, T. Stalcup, J.S. Brooks, Phys. Rev. Lett. 80 (1998) 2453.
[7] S. Hill, S. Maccagnano, K. Park, R.M. Achey, J.M. North, N.S. Dalal, Phys. Rev. B 65 (2002) 224410.
[8] S. Hill, R.S. Edwards, S.I. Jones, J.M. North, N.S. Dalal, Phys. Rev. Lett. 90 (2003) 17204.
[9] E. del Barco, A.D. Kent, S. Hill, J.M. North, N.S. Dalal, E.M. Rumberger, D.N. Hendrickson, N. Chakov, G. Christou, J. Low Temp. Phys. 140 (2005) 119.
[10] A.L. Barra, D. Gatteschi, R. Sessoli, Chem. Eur. J 6 (2000) 1608.